

The Kinematics and Physical Conditions of the Ionized Gas in Markarian 509. II. STIS Echelle Observations.¹

S. B. Kraemer², D. M. Crenshaw³, T. Yaqoob^{4,6}, B. McKernan⁴, J.R. Gabel², I.M.
George^{5,6}, T.J. Turner^{5,6}, & J.P. Dunn³

Received _____; accepted _____

submitted to *The Astrophysical Journal*

¹Based on observations made with the NASA/ESA Hubble Space Telescope. STScI is operated by the Association of Universities for Research in Astronomy, Inc. under the NASA contract NAS5-26555.

²Catholic University of America, NASA's Goddard Space Flight Center, Code 681, Greenbelt, MD 20771; stiskraemer@yancey.gsfc.nasa.gov.

³Department of Physics and Astronomy, Georgia State University, One Park Place South SE, Suite 700, Atlanta, GA 30303

⁴Department of Physics and Astronomy, Johns Hopkins University, Baltimore, MD 21218.

⁵Joint Center for Astrophysics, University of Maryland, Baltimore County, 1000 Hilltop circle, Baltimore, MD 21250.

⁶Laboratory for High Energy Astrophysics, NASA's Goddard Space Flight Center, Code 662, Greenbelt, MD 20771.

ABSTRACT

We present observations of the UV absorption lines in the luminous Seyfert 1 galaxy Mrk 509, obtained with the medium resolution ($\lambda/\Delta\lambda \approx 40,000$) echelle gratings of the Space Telescope Imaging Spectrograph on the *Hubble Space Telescope*. The spectra reveal the presence of eight kinematic components of absorption in Ly α , C IV, and N V, at radial velocities of -422 , -328 , -259 , -62 , -22 , $+34$, $+124$, and $+210$ km s $^{-1}$ with respect to an emission-line redshift of $z = 0.03440$, seven of which were detected in an earlier *Far Ultraviolet Spectrographic Explorer (FUSE)* spectrum. The component at -22 km s $^{-1}$ also shows absorption by Si IV. The covering factor and velocity width of the Si IV lines were lower than those of the higher ionization lines for this component, which is evidence for two separate absorbers at this velocity. We have calculated photoionization models to match the UV column densities in each of these components. Using the predicted O VI column densities, we were able to match the O VI profiles observed in the *FUSE* spectrum. Based on our results, none of the UV absorbers can produce the X-ray absorption seen in simultaneous *Chandra* observations; therefore, there must be more highly ionized gas in the radial velocity ranges covered by the UV kinematic components.

Subject headings: galaxies: Seyfert - X-rays: galaxies - ultraviolet: galaxies - galaxies: individual (Mrk 509)

1. Introduction

Since the launch of the *International Ultraviolet Explorer (IUE)*, it has been known that the UV spectra of Seyfert 1 galaxies show absorption lines intrinsic to their nuclei (Ulrich 1988). With the advent of the *Hubble Space Telescope (HST)*, it is now understood that intrinsic absorption is a common phenomenon, present in more than half of the well-studied Seyfert 1 galaxies (Crenshaw et al. 1999). Among those Seyferts that show absorption, high ionization lines such as N V $\lambda\lambda 1238.8, 1242.8$ and C IV $\lambda\lambda 1548.2, 1550.8$ are always present, along with Ly α , while lower ionization lines, such as Si IV $\lambda\lambda 1393.8, 1402.8$ and Mg II $\lambda\lambda 2796.3, 2803.5$, are less common. Typically, the absorption lines are blueshifted (by up to 2100 km s^{-1}) with respect to the systemic velocities of the host galaxies, indicating net radial outflow. Although there are examples of strong UV absorption lines near systemic velocities, some are found in highly inclined host galaxies and, therefore, are most likely formed in gas within the plane of the host galaxy (Crenshaw et al. 2001; Crenshaw et al. 2002). Among the blue-shifted absorbers, the ionic columns are highly variable, which may be the result of changes in response to the ionizing continuum (cf. Krolik & Kriss 1997; Shields & Hamann 1997) or transverse motion (Crenshaw & Kraemer 1999). Variability is suggestive of the proximity of the absorbers to the central active nucleus, since it may result from the high densities, hence short recombination timescales, or high transverse velocities, similar to those inferred for the emission-line gas close to the active nucleus. Based on density constraints, it has been shown that in at least two sources, NGC 4151 and NGC 3516, much of the absorbing gas may lie within a fraction of a parsec from the central source (Kraemer et al. 2001a; Kraemer et al. 2002). Another indication of small radial distances is the low line-of-sight covering factors derived from some UV absorption lines (Kraemer et al. 2002; Gabel et al. 2002). In addition to the UV absorbers, the presence of intrinsic absorption, typically in the form of bound-free edges of O VII and O VIII, has been detected in the X-ray spectra of a similar fraction of Seyfert 1 galaxies (Reynolds 1997;

George et al. 1998). Most recently, spectra obtained with the *Chandra X-ray Observatory* (*CXO*) have revealed that X-ray absorption lines associated with this material are also blue-shifted (Kaastra et al. 2000; Kaspi et al. 2000, 2001). Although it has been argued that some fraction of the UV absorption arises in the same gas responsible for the X-ray absorption (Mathur, Elvis & Wilkes 1995, 1999; Crenshaw & Kraemer 1999; Kriss et al. 2000; Kraemer et al. 2002), the connection between the X-ray and UV absorption is complex. In fact, there is often a wide range in ionization states in gas which may be at the same radial velocities (Kaspi et al. 2002). Further evidence for this is the co-spatial X-ray and optical line emission seen in the narrow-line regions (NLR) of Mrk 3 (Sako et al. 2000), NGC 1068 (Ogle et al. 2002), and NGC 4151 (Ogle et al. 2000).

Mrk 509 is a highly luminous ($L_{h\nu > 13.6eV} \sim 10^{45}$ erg s⁻¹; see Kriss et al. [2000]; Yaqoob et al. [2002a]) Seyfert 1 galaxy. Phillips et al. (1983) determined that the nucleus is surrounded by two distinct components of extended ionized gas: a low ionization component, with a velocities indicative of rotation in the galactic disk, and a high ionization component, with velocities blue-shifted with respect to those in the disk. Phillips et al. suggested that this high ionization component is part of an outflowing shell of gas. If gas is distributed within a bicone centered on the active nucleus, as appears to be the case in other Seyfert galaxies (Crenshaw & Kraemer 2000; Crenshaw et al. 2000; Ruiz et al. 2001), the axis of the outflow must be roughly parallel to our line-of-sight (see Fig. 8 in Phillips et al.). There is extended broad Balmer line emission (FWZI > 15,000 km s⁻¹), presumably scattered light from the unresolved broad line region, in an axisymmetrical distribution surrounding the active nucleus (Mediavilla et al. 1998), consistent with the geometry suggested by Phillips et al. (1983). Based on recent X-ray observations of Mrk 509 with *XMM-Newton*, Pounds et al. (2001) argued that the inclination of the putative accretion disk within the active nucleus is < 30°, which also fits with the proposed geometry.

Two kinematic components of intrinsic Ly α and C IV absorption, at ~ -420 and $+40$ km s $^{-1}$, were detected by York et al. (1984) in high-dispersion *IUE* spectra of Mrk 509. In their *HST*/Faint Object Spectrograph observations ~ 12 yr later, Crenshaw, Bogges, & Wu (1995) found the same components, as well as N V absorption at these velocities. York et al. (1984) and Crenshaw et al. (1995) suggested that these lines formed in extended regions of ionized gas in the host galaxy. Kriss et al. (2000) obtained a high resolution ($\lambda/\Delta\lambda \approx 15,000$) *Far Ultraviolet Spectroscopic Explorer (FUSE)* spectrum over the wavelength range 915 – 1185 Å on 1999 November 9, 11 that shows intrinsic absorption in the lines of O VI $\lambda\lambda 1031.9, 1037.6$, C III $\lambda 977.0$, and the H I Lyman lines, consisting of seven, relatively narrow (FWHM ≤ 63 km s $^{-1}$), kinematic components which are clustered into two groups, at -370 km s $^{-1}$ and near the systemic velocity. They suggested that the former was associated with the extended, blue-shifted ionized gas observed by Phillips et al. (1983). In addition to the UV absorption, *ASCA* spectra showed strong evidence for the presence of an X-ray warm absorber (Reynolds 1997; George et al. 1998).

We have obtained simultaneous *CXO*/High Energy Transmission Grating (HETG) and *HST*/Space Telescope Imaging Spectrograph (STIS) medium resolution spectra of Mrk 509 on 2001 April 13. We note that there are no previous *HST* high-resolution ($\lambda/\Delta\lambda \geq 10,000$) UV spectra, except for a Goddard High-Resolution Spectrograph (GHRS) observation of the intrinsic L α absorption (Crenshaw et al. 1999), which is highly saturated (see section 2.2). The analysis of the X-ray spectra are discussed in Yaqoob et al. (2002a) and Yaqoob et al. (2002b; hereafter Paper I). In Paper I, we describe the details of the ionizing continuum and the physical nature of the X-ray warm absorbing gas, including model predictions of ionic column densities. In the present paper, we present our analysis of the STIS spectra and the results of photoionization modeling of the UV absorbers. The paper is organized as follows: in Section 2 we describe the observations, and give the details of the measurement of the intrinsic lines, in Section 3 we detail the photoionization modeling of the absorbers,

in Section 4 we discuss the implications of the result, and Section 5 gives our summary.

2. Observations and Data Analysis

2.1. New STIS Observations

We obtained STIS echelle spectra of the nucleus of Mrk 509 through a $0''.2 \times 0''.2$ aperture on 2001 April 13. The details of these observations are listed in Table 1. We reduced the STIS spectra using the IDL software developed at NASA’s Goddard Space Flight Center for the STIS Instrument Definition Team. The data reduction includes a procedure to remove the background light from each order using a scattered light model devised by Lindler (1998). The individual orders in each echelle spectrum were spliced together in the regions of overlap.

Figure 1 shows portions of the STIS spectra where intrinsic absorption is detected in the UV. The spectra are normalized (as described below) and are plotted as a function of the radial velocity, relative to a systemic redshift of $z = 0.03440$ from the optical emission lines (Crenshaw et al. 1999), since H I 21-cm measurements are not available. We have adopted the numbering of components given by Kriss et al. (2000). Each of their components is present in N V $\lambda\lambda$ 1238.8, 1242.2 and C IV λ 1548.2, 1550.8, and we identify a new component (4′) in the blue wing of component 4; the new detection is likely due to the higher spectral resolution of STIS. Although these components are completely saturated and blended together in Ly α , they are all undoubtedly present, since they are present and resolved in the *FUSE* spectra of Ly β . We have also detected Si IV $\lambda\lambda$ 1393.8, 1402.8 in component 4, but not in any other component. We have not detected lower ionization lines (e.g., Si III λ 1206.5, C II λ 1334.5, Mg II $\lambda\lambda$ 2796.3, 2803.5) in any component in the STIS spectra.

Figure 1 shows that the absorption components are clustered in two groups in radial velocity; components 2 and 4 from the two clusters are the strongest in the high-ionization lines of C IV and N V. None of the components is highly saturated, since the long-wavelength member of each doublet is clearly not as deep as the short-wavelength member (which has twice the oscillator strength) in each case. The saturated Ly α absorption covers the same velocity range as these two clusters, and there is no evidence for H I absorption outside of the two clusters. We note that our velocity scale is offset from that of Kriss et al. (2000) by 52 km s⁻¹; they use a systemic redshift of $z = 0.03457$ ($cz = 10,365$ km s⁻¹) from the nuclear [O III] emission in Phillips et al. (1993), whereas we use a systemic redshift of $z = 0.03440$ ($cz = 10,313$ km s⁻¹) to be consistent with our earlier measurements (Crenshaw et al. 1995, 1999). We note that components 5 – 7 are not necessarily redshifted with respect to the host galaxy, since there is a tendency for the [O III] $\lambda\lambda$ 4959, 5007 emission in Seyfert 1 galaxies to be slightly blueshifted with respect to the systemic velocity determined from H I 21-cm emission (Crenshaw et al. 1999).

2.2. Measurements and Observational Results

The procedures we used to measure the intrinsic absorption lines follow those of Crenshaw et al. (1999). To determine the shape of the underlying emission, we fit a cubic spline to regions on either side of the absorption, and then normalized the absorption profiles by dividing the observed spectra by the spline fits. We determined the covering factor C_{los} , which is the fraction of continuum plus emission that is occulted by the absorber in our line of sight, using the technique of Hamann et al. (1997) for doublets. Due to the modest signal-to-noise of the spectra and problems with blending of the components, we can only determine C_{los} reliably in the cores of the strongest, relatively unblended lines. Thus, we used both C IV and N V doublets to determine C_{los} for the cores of components

1, 2, 4, and 6. To determine the column densities, we converted each normalized profile to optical depth as a function of radial velocity, and integrated across the profile, as described in Crenshaw et al. (1999). For the components with strong evidence for nonunity covering factors, we determined the true optical depths using the measured C_{los} values and the formalism of Hamann et al. (1997). For the other components, we assumed $C_{los} = 1$.

Table 2 gives the measured radial velocity centroids, widths (FWHM), covering factors, and associated one-sigma errors for each kinematic component. These values represent the means and standard deviations determined from the measurements of the individual C IV and N V profiles. For component 4, the Si IV profiles yield a very different width and covering factor compared to the C IV and N V profiles. We take this as an indication that there are two different physical components at this radial velocity, which we call “4 (high)” and “4 (low)”, for high- and low-ionization components, respectively.

The covering factors for components 4 (high) and 6 are consistent with a value of one, although we cannot rule out the possibility that they are slightly lower. Components 1, 2, and 4 (low) all show strong evidence for a nonunity covering factor, whereas the covering factors for the weaker components 3, 4', 5, and 7 cannot be reliably determined. Unocculted emission from the narrow-line region (NLR) in this small aperture cannot explain the nonunity covering factors, since this emission would be centered near zero velocity and would decrease away from line center. The simplest explanation for the partial covering is that the absorbers associated with components 1, 2, and 4 (low) are not occulting the entire continuum source and/or broad-line region (BLR) as seen in projection on the sky.

We list the ionic column densities for each component in Table 3. Components 4 (high) and 4 (low) required special treatment. For component 4 (low), our photoionization models indicate very large columns of C IV and N V (Section 3.2). To see if these columns were consistent with the observed profiles, we simulated the C IV and N V profiles by assuming

the same profile and covering factor as those for Si IV ($C_{los} = 0.32$). The simulated C IV and N V profiles are plotted in Figure 1, and demonstrate that the large columns for component 4 (low) in Table 6 can indeed be hidden in the observed profiles. However, column densities spanning a wide range of values could be hidden, due to the small covering factor of this component, and so we have no observationally determined values for component 4 (low) in Table 3. To determine the column densities for component 4 (high), we assumed that the C IV and N V lines for component 4 (low) were indeed saturated, and therefore form pedestals from which the component 4 (high) optical depths can be measured against.

2.3. The Far-UV Light Curve of Mrk 509

To place the STIS observations in context with previous far-UV observations, we have retrieved all of the previous low-resolution spectra of Mrk 509 obtained in the far-UV. Table 4 lists these spectra (i.e., those not listed in Table 1), which were obtained by the *IUE*, the Hopkins Ultraviolet Telescope (*HUT*), and *HST*/FOS. We retrieved the most recently processed versions of these spectra from the Multimission Archive at STScI. We measured their continuum fluxes by averaging the points in a bin centered at 1385 Å (observed frame) with a width of 40 Å. We determined the one-sigma flux errors from the standard deviations of the averages; for the *IUE* spectra, this technique is known to overestimate the errors (Clavel et al. 1991), and we scaled the errors for these observations by a factor of 0.5 to ensure that observations taken on the same day agreed to within the errors (on average).

Figure 2 shows that the far-UV continuum of Mrk 509 varied dramatically over a span of 23 years. The continuum light curve is clearly undersampled, as evidenced by the large variations over ~ 60 days near JD 2,448,200. It can be seen that the STIS observation was obtained when the far-UV continuum was in a low state: $F_{\lambda}(1385\text{\AA}) = 5.3 (\pm 0.4) \times 10^{-14}$ ergs s $^{-1}$ cm $^{-2}$ Å $^{-1}$. Interestingly, the simultaneous *CXO* observations show that

Mrk 509 was in an average X-ray state at this time (Yaqoob et al. 2002a). Although the *FUSE* observation does not contain this wavelength region, we can compare it with our STIS observation by looking at the continuum in the region of overlap. At 1180 Å, the continuum fluxes are 6.0 (± 0.7) and 6.2 (± 1.0) $\times 10^{-14}$ ergs s $^{-1}$ cm $^{-2}$ Å $^{-1}$ for the *FUSE* and STIS spectra, respectively, indicating that these spectra were taken in a similar low state. It would be interesting to obtain STIS observations of Mrk 509 in a high state, given strong evidence for absorption variations in response to continuum changes in NGC 4151 (Kraemer et al. 2001a) and NGC 3516 (Kraemer et al. 2002).

3. Photoionization Models

3.1. Inputs to the Photoionization Models

Photoionization models for this study were generated using the code CLOUDY90⁷ (Ferland et al. 1998). We have modeled the absorbers as matter-bounded slabs of atomic gas, irradiated by the ionizing continuum radiation emitted by the central source. As per convention, the models are parameterized in terms of the ionization parameter,

$$U = \frac{1}{4\pi r^2 n_H c} \int_{\nu_0}^{\infty} \frac{L_\nu}{h\nu} d\nu, \quad (1)$$

where L_ν is the frequency dependent luminosity of the ionizing continuum, r is the distance between the cloud and the ionizing source and $h\nu_0 = 13.6$ eV, and n_H is the number density of hydrogen atoms at the illuminated face of the slab (note that, in general, r and n_H cannot be determined independently in absorption line studies). The models are also

⁷The X-ray models described in Paper I were generated with the code XSTAR; we found no significant differences in the ionic column densities predicted by the two codes.

parameterized in terms of the total hydrogen column density, $N_{\text{H}} (= N_{\text{H I}} + N_{\text{H II}})^8$. For the models, we have assumed only thermal broadening, since the absorption lines are quite narrow (see Table 2) and widths greater than thermal (which are \sim a few km s^{-1}) are likely to be due to the superposition of unresolved kinematic components (note that the resolution of the STIS E140M echelle grating is $\sim 7 \text{ km s}^{-1}$ at 1550 \AA). The details of the ionizing continuum and element abundances assumed for these models are given in Paper I. The absorbing gas is assumed to be free of cosmic dust.

3.2. Model Results

The “best-fit” values of U and N_{H} (determined by matching the measured values of $N_{\text{N V}}$, $N_{\text{C IV}}$ and $N_{\text{Si IV}}$) for the models are listed in Table 5, and the predicted ionic column densities are given in Table 6. Based on the models, none of the UV absorbers has a sufficient column density to significantly modify the intrinsic continuum at wavelengths above the Lyman limit. Hence, even though several of the components have covering fractions near unity, there will be no strong effects due to the screening of one component by another. For components 1, 2, 3, 4', 5, 6, and 7, the models match the observed $N_{\text{N V}}$ and $N_{\text{C IV}}$ to well within the measurement errors. Our predictions for $N_{\text{C III}}$ for these components are in good agreement with Kriss et al. (2000), with the exception of a factor of ~ 8 underprediction for component 1 and a factor of ~ 2 overprediction for component 3. The latter is likely to the different line widths assumed for this component, while the discrepancy for component 1 may be evidence for a second low ionization component at this velocity (also, see Fig. 2 in Kriss et al. [2000]). The models also underpredict $N_{\text{H I}}$ for

⁸We use N_{XM} to denote the ionic column density, where “X” is the atomic symbol and “M” is the ionization state.

components 1, 3, 5, 6, and 7. However, the additional H I columns may arise in the X-ray absorber (see Section 3.3).

For the low ionization fraction of component 4, the model predictions match the measured value for $N_{\text{Si IV}}$ and the upper limits for $N_{\text{Si III}}$ and $N_{\text{C II}}$. As noted in Section 2.2, the model predictions for $N_{\text{C IV}}$ and $N_{\text{N V}}$ for the low ionization component were then used to determine the respective columns from the high ionization gas associated with component 4, which we were then able to model successfully. The large H I column predicted by the low ionization component is in rough agreement with that derived from Ly β by Kriss et al. (2000), which suggests that the low ionization gas covers the UV continuum source but not the BLR clouds (which contribute a negligible amount of Ly β emission; see discussion in Gabel et al. [2002]). Although the low ionization model predicts $N_{\text{C III}} \sim 30$ times greater than that derived by Kriss et al. (2000), the apparent discrepancy is clearly due to large covering factor assumed by those authors ($C_{\text{los}} = 0.92$), which is appropriate for the high ionization component but not the gas in which the C III line forms.

Our model predictions for the O VI column densities are much larger than those measured by Kriss et al. (2000) for components 1, 3, 4, by factors of 3 – 12, and lower in component 5 by a factor of 4. Of course, this could be the result of variability in these components, but we consider that unlikely, given that the *FUSE* and *HST*/STIS observations were obtained at a similar continuum state. Inspection of the *FUSE* O VI profiles shows that they are highly saturated, and the components could potentially harbor much larger columns than those measured by Kriss et al. To test the compatibility of our model predictions with the *FUSE* observation, we have generated a simulated O VI $\lambda 1031.9$ profile in the following manner. First, we isolated the optical depth profile of each kinematic component in N V $\lambda 1238.8$. Then, we scaled each profile so that they would yield the predicted O VI columns from our models. Finally, we combined the optical depths

and converted them to normalized flux (as a function of radial velocity) using the covering factors of each component given by Kriss et al. There are two reasons for using the Kriss et al. covering factors, rather than the ones we have determined. First, it is possible for two absorption lines to have different covering factors, even if they come from the same gas, due to different contributions to the underlying emission from the continuum source and BLR (for a demonstration of this effect, see Gabel et al. [2002]). Second, the *FUSE* aperture (30" x 30") is much larger than the STIS aperture that we used (0".2 x 0".2), and it is possible that more unocculted emission (e.g., from the NLR, a scattering region, or hot stars in the host galaxy) is admitted by the large aperture, which could contribute to the difference in the derived covering factors at low radial velocities, particularly for components 4 (high ionization) and 6.

Our simulated O VI profile is shown in Figure 3. Comparison with Figure 2 in Kriss et al. (2000) shows that it provides a very good match to the observed O VI $\lambda 1031.9$ profile. There is a small discrepancy in that the flux between components 5 and 6 is a little high in the simulated profile, but that could be due to a slight underestimate of the N V optical depth in the wings of these components. We conclude that a direct comparison of model and observed O VI column densities is not feasible, due to heavy saturation of the absorption components, but that the O VI column densities from our models are at least consistent with the observed O VI profile.

3.3. The Nature of the UV Absorbers

Based on our model predictions, the components of UV absorption in Mrk 509 have smaller column densities and are, on average, in a lower state of ionization than the strongest components in the Seyfert 1 galaxies NGC 5548 ($\log U = -0.62$, $N_{\text{H}} = 2.0 \times 10^{20} \text{ cm}^{-2}$; Crenshaw et al. 2002, in preparation), NGC 3783 ($\log U = -0.19$, $N_{\text{H}} = 1.5 \times$

10^{21} cm^{-2} ; Kraemer et al. 2001b), and NGC 3516 ($\log U = -0.72$, $N_{\text{H}} = 1.4 \times 10^{21} \text{ cm}^{-2}$; Kraemer et al. 2002). Interestingly, they are similar in column density and FWHM to the weak, narrow components detected in NGC 4151, which we had determined were at least tens of pcs from the central source (Kraemer et al. 2001a). The combination of high and low ionization absorbers within a single kinematic component (component 4) has been seen in NGC 3783 (Kraemer et al. 2001b; Gabel et al. 2002) and NGC 3516 (Kraemer et al. 2002). If these components are at the same radial distance, there must be density inhomogeneities within the absorbing gas, with the lower ionization absorption occurring in denser gas. The fact that the low ionization component has a lower covering factor than the high ionization component is also evidence for different densities, since the denser component is likely more compact.

Since, summed over the eight model kinematic components, the total N_{OVII} is $= 3.2 \times 10^{16} \text{ cm}^{-2}$, or about 10% of the total observed O VII column, none of the UV absorbers can be identified with the X-ray absorbing gas described in Paper I. This is contrary to the suggestion by Kriss et al. (2000) that, based on the large O VI column, component 5 must strongly contribute to the X-ray absorption. However, as discussed in Section 3.2, the O VI column predicted by our models is consistent with the *FUSE* spectrum. Also, a model with physical parameters determined by Kriss et al. (2000) for this component ($\log U = -0.43$, $N_{\text{H}} = 5.0 \times 10^{20} \text{ cm}^{-2}$) predicts a N V column of $\sim 10^{15} \text{ cm}^{-2}$, which is clearly inconsistent with the STIS spectrum. The discrepancy may result from the difficulty in deriving accurate lower limits to column densities from such heavily saturated lines.

Models of the X-ray absorber (Paper I) predict detectable C IV and N V column densities of $1.2 \times 10^{13} \text{ cm}^{-2}$ and $8.5 \times 10^{13} \text{ cm}^{-2}$, respectively. However, as discussed above, our models of the UV components, which assume a single physical component for each (except for component 4), do not predict substantial X-ray absorption. Thus, the UV

columns associated with the X-ray absorber are likely to be “hidden” in one or more of the UV components. If the X-ray absorber is coincident with only one UV component, the C IV column could be hidden in any kinematic component, but the N V column could only be hidden in components 1, 2, 4', or 4. Alternatively, the C IV and N V columns from the X-ray absorber could be spread out amongst some or all of the kinematic components. Thus, it is clear that the X-ray absorption occurs within the velocity ranges covered by the two clusters of UV absorption, since otherwise we would have uniquely detected its UV columns. The velocity coverage of the X-ray absorption in the *CXO* spectrum is consistent with this conclusion (Paper I). The Ly α profile in Figure 1 is also consistent with the conclusion that the X-ray absorption must fall in the velocity ranges covered by the UV absorbers, since we expect a substantial H I column from the X-ray absorber ($1.4 \times 10^{15} \text{ cm}^{-2}$, see Paper I), and yet we see no H I absorption in the Ly α profile (Figure 1) that is outside of the two clusters of UV absorption. Based on the *FUSE* spectra, Kriss et al. (2000) derived a total $N_{\text{H I}} \approx 4.7 \times 10^{15} \text{ cm}^{-2}$ (excluding component 4, in which the Ly β line may form principally in the low ionization component). The UV models predict a total $N_{\text{H I}} = 1.6 \times 10^{15} \text{ cm}^{-2}$ (excluding components 4 and 4'), which leaves $3.1 \times 10^{15} \text{ cm}^{-2}$ unaccounted for. This is roughly consistent with the X-ray model prediction, and further evidence for additional gas at the same velocities of a number of the UV components. It is interesting that there is also strong evidence for a wide range in ionization state at the same velocities in the intrinsic UV and X-ray absorbers in the Seyfert 1 galaxy NGC 3783 (Kaspi et al. 2002).

4. Discussion

In general, intrinsic UV (Crenshaw et al. 1999) and X-ray (Kaspi et al. 2000, 2001; Kaastra et al. 2000) absorption lines detected in Seyfert 1 galaxies are blue-shifted,

indicative of radial outflow. However, in the case of Mrk 509, the clustering of component velocities near systemic and the presence of red-shifted gas (although this is somewhat uncertain; see Section 2.1) differ from the more obvious cases of radial outflow discussed by Crenshaw et al. (1999). Kriss et al. (2000) suggested that this may be the result of the absorbers at radial distances of ~ 300 pc, co-located with the low ionization gas detected by Phillips et al. (1983) and moving primarily transversely to our line-of-sight. Indeed, it has been suggested that UV absorption lines form in disk-driven winds (e.g., Proga, Stone, & Kallman 2000). If this is the case, the low velocities we observe in Mrk 509 require a viewing angle roughly orthogonal to the direction of the flow, similar to the geometry suggested by Kriss et al. (2000). This scenario is consistent with the evidence that the accretion disk in Mrk 509 is viewed roughly face-on (Pounds et al. 2001). If the widths of the UV absorption lines detected in Seyfert 1s are the result of superposition of multiple kinematic components, viewing an outflow stream from this vantage point might help explain the narrowness of the lines seen in Mrk 509. Nevertheless, there are some problems with this hypothesis. Since Mrk 509 is a high luminosity Seyfert 1, disk-wind models predict that the outflow will be more confined to the disk than in lower luminosity AGN (Konigl & Kartje 1994; Murray et al. 1995). The axisymmetric distribution of the reflected broad Balmer line emission in Mrk 509 can be interpreted as evidence for an obscuring torus or wind that covers only a small solid angle (Mediavilla et al. 1998), which is consistent with a “flattened” wind. However, most of the UV components have covering factors near unity, which may be difficult to achieve with a flattened wind viewed against a roughly face-on disk, depending on the location of the continuum source relative to the base of the wind. Specifically, the “launch-pad” of the wind must be *interior* to the UV continuum source.

Alternatively, it is possible that the observed velocities of the UV absorbers are close to their true radial velocities. In this case, the absorbers may not be part of a disk-driven flow and are, instead, gas that has been elevated off the disk and, therefore, may be more likely

to occult the continuum and BLR when the disk is viewed face-on. Although disk-wind models include such a component, both the X-ray and UV absorbers detected in Mrk 509 are too neutral to be the “hitch-hiker” gas proposed by Murray et al. (1995) to shield the disk-driven winds or the highly-ionized gas in the inner part of the wind modeled by Proga et al. (2000), since, in both cases, these components may have ionization parameters ≥ 10 . Krolik & Kriss (1995) proposed that UV absorbers are high density knots embedded in a thermally expanding, highly ionized wind, which would provide a natural explanation for the kinematic association of the UV and X-ray absorbers. However, this model predicts radial velocities similar to the disk-driven winds ($>$ several hundred km s^{-1}), hence would still require a special geometry to explain the low radial velocities and large values of C_{los} . A simpler scenario would have the absorbers at large radial distances, e.g. 100’s of pcs as suggested by Kriss et al. (2000). As noted in Section 3.3, similar UV absorbers were found at large distances in NGC 4151 (Kraemer et al. 2001a). Furthermore, studies of the narrow-line region kinematics indicate a strong drop in radial velocities in emission-line gas at distances $>$ few hundred pcs (Crenshaw & Kraemer 2000; Crenshaw et al. 2000; Ruiz et al. 2001), so it is not necessarily surprising that the absorbers within the NLR would have similar kinematics. However, better determination of the radial distances of these absorbers requires constraints on the gas density, which can only be achieved via variability studies.

5. Summary

We have used UV medium resolution echelle spectra obtained with *HST*/STIS and X-ray spectra obtained with *CXO*/HETG to study the physical conditions in the intrinsic absorbers in the Seyfert 1 galaxy Mrk 509. The analysis of the X-ray warm absorber is given in Paper I, while here we describe the nature of the UV absorbers. We have determined the following:

1. We have detected 8 separate kinematic components in Ly α , C IV, and N V, seven of which were previously detected in a *FUSE* spectrum. Component 4 also shows the presence of Si IV. We derived a $C_{los} \approx 0.32$ from the Si IV lines, as opposed to ≈ 0.98 from the high ionization lines, which we interpret as evidence for two separate physical components at this velocity, similar to that observed in NGC 3783 (Kraemer et al. 2001b) and NGC 3516 (Kraemer et al. 2002).

2. Contrary to the analysis in Kriss et al. (2000), none of the UV absorbers possesses a sufficiently high column density or ionization parameter to be identified with the X-ray warm absorber. However, based on the warm absorber models presented in Paper I, it is likely that highly ionized gas is kinematically associated with one or more of the UV components.

3. There is evidence suggesting that accretion disk in Mrk 509 is viewed roughly face-on. Although disk-wind models would predict low velocities for the UV absorbers with this geometry, it is clear that they cannot account for the large covering factors derived for several of the components. Alternatively, the properties of the absorbers may be consistent with outflow perpendicular to the surface of a disk. Furthermore, it is plausible that the absorbers lie within the NLR of Mrk 509, at significant radial distances from the central source, and hence a part of a different population of intrinsic absorbers than that detected in several other Seyfert 1 galaxies. The UV continuum is currently in a low-state, while the X-ray continuum flux is near its historical average (Yaqoob et al. 2002a); therefore spectra taken as the source brightens (over a timeframe of several yrs) will provide a means to constrain the densities and, thus, the radial distances of the absorbers.

Support for proposal 8877 was provided by NASA through a grant from the Space Telescope Science Institute, which is operated by the Association of Universities for Research in Astronomy, Inc., under NASA contract NAS 5-26555. Some of the data presented in

this paper were obtained from the Multimission Archive at the Space Telescope Science Institute (MAST). Support for MAST for non-HST data is provided by the NASA Office of Space Science via grant NAG5-7584 and by other grants and contracts. We would like to thank Jose Ruiz for useful discussions. We thank an anonymous referee for their comments.

REFERENCES

- Clavel, J., et al. 1991, *ApJ*, 366, 64
- Crenshaw, D.M., Maran, S.P., & Mushotzky, R.F. 1998, *ApJ*, 496, 797
- Crenshaw, D.M., & Kraemer, S.B. 1999, *ApJ*, 521, 572
- Crenshaw, D.M., & Kraemer, S.B. 2000, *ApJ*, 532, L101
- Crenshaw, D.M., Kraemer, S.B., Boggess, A., Maran, S.P., Mushotzky, R.F., & Wu, C.-C. 1999, *ApJ*, 516, 750
- Crenshaw, D.M., Kraemer, S.B., Bruhweiler, F.C., & Ruiz, J.R. 2001, *ApJ*, 555, 633
- Crenshaw, D.M., et al. 2000, *AJ*, 120, 1731
- Crenshaw, D.M., et al. 2002, *ApJ*, 566, 187
- Ferland, G.J. et al. 1998, *PASP*, 110, 761
- Gabel, J.R., et al. 2002, *ApJ*, in press
- George, I.M., Turner, T.J., Netzer, H., Nandra, K., Mushotzky, R.F., & Yaqoob, T. 1998a, *ApJS*, 114, 73
- Hamann, F., Barlow, T.A., Junkkarinen, V., & Burbidge, E. M. 1997, *ApJ*, 478, 80
- Kaastra, J.S., Mewe, R., Liedahl, D.A., Komossa, S., & Brinkman, A.C. 2000, *A&A*, 354, L83
- Kaspi, S., Brandt, W.N., Netzer, H., Sambruna, R., Chartas, G., Garmire, G.P., & Nousek, J.A. 2000, *ApJ*, 535, L17 (K2000)
- Kaspi, S., et al. 2001, *ApJ*, 554, 216
- Kaspi, S., et al. 2002, *ApJ*, in press
- Konigl, A., & Kartje, J.F. 1994, *ApJ*, 434, 446

- Kraemer, S.B., Crenshaw, D.M., & Gabel, J.R. 2001b, *ApJ*, 557, 30
- Kraemer, S.B., et al. 2001a, *ApJ*, 551, 671
- Kraemer, S.B., et al. 2002, *ApJ*, in press
- Kriss, G.A., et al. 2000, *ApJ*, 538, L17
- Krolik, J.H., & Kriss, G.A. 1995, *ApJ*, 447, 512
- Krolik, J.H., & Kriss, G.A. 1997, in *Mass Ejection from Active Galactic Nuclei*, ed. N. Arav, I. Shlosmann, & R.J. Weymann (San Francisco: Astronomical Society of the Pacific), ASP Conference Series, 128, 132
- Lindler, D. 1998, *CALSTIS Reference Guide (CALSTIS Version 5.1)*
- Mathur, S., Elvis, M., & Wilkes, B.J. 1999, *ApJ*, 519, 605
- Mathur, S., Elvis, M., & Wilkes, B.J. 1995, *ApJ*, 452, 230
- Mediavilla, E., Arribas, S., Garcia-Lorenzo, B., & del Burgo, C. 1998, *ApJ*, 494, L9
- Murray, N., Chiang, J., Grossman, S.A., & Voigt, G.M. 1995, *ApJ*, 451, 498
- Ogle, P.M., Marshall, H.L., Lee, J.C., & Canizares, C.R. 2000, *ApJ*, 545, L81
- Ogle, P.M., Canizares, C.R., Dewey, D., Lee, J.C., & Marshall, H.L. 2002, in *Mass Outflow from Active Galactic Nuclei*, ed. D.M. Crenshaw, S.B. Kraemer, & I.M. George (San Francisco: Astronomical Society of the Pacific), ASP Conference Series, 255, 13
- Phillips, M.M., Baldwin, J.A., Atwood, B., & Carswell, R.F. 1993, *ApJ*, 274, 558
- Pounds, K.A., Reeves, J., O'Brien, P., Page, K., Turner, M., & Nayakshin, S. 2001, *ApJ*, 559, 181
- Proga, D., Stone, J.M., & Kallman, T.R. 2000, *ApJ*, 543, 686
- Reynolds, C.S. 1997, *MNRAS*, 286, 513

- Ruiz, J.R., Crenshaw, D.M., Kraemer, S.B., Bower, G.A., Gull, T.R., Hutchings, J.B.,
Kaiser, M.E., & Weistrop, D. 2001, AJ, 122, 2961
- Sako, M., Kahn, S.M., Paerels, F., & Liedahl, D.A. 2000, ApJ, 543, L115
- Shields, J.C., & Hamann, F. 1997, ApJ, 481, 752
- Ulrich, M.-H. 1988, MNRAS, 230, 121
- Yaqoob, Y., McKernan, B., Kraemer, S.B., Crenshaw, D.M., Gabel, J.R., George, I.M., &
Turner, T.J. 2002b, submitted to ApJ (Paper I)
- Yaqoob, T., Pradmanabhan, U., McKernan, B., Kraemer, S.B., George, I.M., Turner, T.J.,
& Crenshaw, D.M. 2002a, ApJ, in press
- York, D.G., Ratcliff, S., Blades, J.C., Cowie, L.L., Morton, D.C., & Wu, C.-C. 1984, ApJ,
276, 92

Fig. 1.— Portions of the STIS echelle spectra of Mrk 509, showing the intrinsic absorption lines in different ions. Normalized fluxes are plotted as a function of radial velocity, relative to an emission-line redshift of $z = 0.03440$. For the doublets, the short wavelength member is plotted in blue, and the long wavelength member is plotted in red. The kinematic components are identified with vertical dotted lines at their measured positions. Areas where a component from one doublet member are heavily contaminated by another component from the other member are plotted as dotted lines. Simulated N V and C IV profiles for component 4 (low), as described in the text, are plotted in green.

Fig. 2.— Far-UV continuum light curve of Mrk 509. Fluxes (in 10^{-14} ergs s^{-1} cm^{-2} \AA^{-1}) at 1385 \AA are plotted as a function of Julian date. The pluses are from *IUE*, and the X's are from the other satellites; vertical lines indicate the error bars (\pm one σ).

Fig. 3.— Simulated O VI $\lambda 1031.9$ profile, based on the optical depth profiles from N V, the covering factors of Kriss et al. (2000), and the predicted O VI columns from the model of each component, as described in the text. The normalized flux is plotted as a function of radial velocity, relative to an emission-line redshift of $z = 0.03440$.

Table 1. *HST*/STIS High-Resolution Spectra of Mrk 509

Instrument	Grating	Coverage (Å)	Resolution ($\lambda/\Delta\lambda$)	Exposure (sec)	Date (UT)
STIS	E140M	1150 – 1730	46,000	7600	2001 April 13
STIS	E230M	2275 – 3120	30,000	2700	2001 April 13

Table 2. Absorption Components in Mrk 509

Comp.	Velocity ^a (km s ⁻¹)	FWHM (km s ⁻¹)	C _{los} ^b
1	-422 (±2)	28 (±6)	0.52 (±0.05)
2	-328 (±2)	49 (±8)	0.91 (±0.06)
3	-259 (±2)	41 (±2)	—————
4'	-62 (±2)	32 (±3)	—————
4 (high)	-22 (±1)	52 (±5)	0.98 (±0.06)
4 (low)	-21 (±2) ^c	21 (±3) ^c	0.32 (±0.03) ^c
5	+34 (±2)	35 (±3)	—————
6	+124 (±3)	29 (±6)	1.02 (±0.04)
7	+210 (±11)	53 (±9)	—————

^aVelocity centroid for a systemic redshift of $z = 0.03440$.

^bCovering factor in the line of sight.

^cDetermined from Si IV, rather than N V and C IV.

Table 3. Measured Ionic Column Densities (10^{14} cm^{-2})

Comp.	N V	C IV	Si IV	Si III	C II
1	1.16 ± 0.19	0.70 ± 0.10	<0.03	<0.01	<0.05
2	2.40 ± 0.19	2.78 ± 0.29	<0.03	<0.01	<0.05
3	0.58 ± 0.10	0.92 ± 0.33	<0.03	<0.01	<0.05
4'	0.84 ± 0.17	0.81 ± 0.08	<0.03	<0.01	<0.05
4 (high)	1.67 ± 0.20	1.32 ± 0.32	<0.03	<0.01	<0.05
4 (low)	————	————	0.21 ± 0.05	<0.05	<0.20
5	0.43 ± 0.10	0.29 ± 0.07	<0.03	<0.01	<0.05
6	0.63 ± 0.10	0.39 ± 0.05	<0.03	<0.01	<0.05
7	0.36 ± 0.09	0.10 ± 0.03	<0.03	<0.01	<0.05

Table 4. Low-Resolution FUV Spectra of Mrk 509

Instrument/ Grating	Coverage (\AA)	Resolution ($\lambda/\Delta\lambda$)	Date (UT)
IUE SWP	1150 – 1978	~ 250	1978 June 7 – 1993 November 9 ^a
FOS G130H	1150 – 1605	~ 1200	1992 June 21
HUT	820 – 1840	~ 450	1995 March 16

^aSee the IUE Merged Log at <http://archive.stsci.edu/iue>.

Table 5. Photoionization Model Parameters

Comp.	N_H (cm^{-2})	$\log(U)$	$\log(\xi)^a$
1	1.03×10^{19}	-0.82	0.67
2	8.30×10^{18}	-1.31	0.18
3	1.77×10^{18}	-1.48	0.01
4'	3.40×10^{18}	-1.19	0.30
4 (high)	9.35×10^{18}	-1.02	0.47
4 (low)	3.40×10^{19}	-1.70	-0.21
5	3.86×10^{18}	-0.82	0.67
6	6.20×10^{18}	-0.78	0.71
7	4.00×10^{19}	-0.16	1.33

^a For comparison to XSTAR models (see Paper I), we also list the ionization parameter $\xi = \frac{1}{r^2 n_H} \int_{\nu_0}^{13.6\text{keV}} L_\nu d\nu$. Based on the model SED, $\xi = (0.0321)U$.

Table 6. Predicted Ionic Column Densities^a (10^{14} cm^{-2})

Comp.	H I	O VI	N V	C IV	Si IV	C III	Si III	C II
1	2.58	22.9	1.16	0.75	–	0.02	–	–
	(5.70)	(1.90)	(1.16)	(0.70)	(<0.03)	(0.16)	(<0.01)	(<0.05)
2	7.25	20.2	2.40	2.77	–	0.26	–	–
	(5.30)	(13.0)	(2.40)	(2.78)	(<0.03)	(0.24)	(<0.01)	(<0.05)
3	2.39	3.35	0.59	0.91	–	0.13	–	–
	(9.30)	(1.20)	(0.58)	(0.92)	(<0.03)	(0.05)	(<0.01)	(<0.05)
4'	2.22	9.02	0.84	0.82	–	0.06	–	–
			(0.82)	(0.81)	(<0.03)		(<0.01)	(<0.05)
4 (high)	3.87	24.8	1.67	1.33	–	0.06	–	–
	–	(12.0)	(1.67)	(1.32)	–	–	–	–
4 (low)	78.1	36.9	11.0	28.3	0.21	6.58	0.05	0.07
	(60.0)	–	–	–	(0.21)	(0.21)	(<0.05)	(<0.20)
5	0.97	8.60	0.43	0.28	–	0.01	–	–
	(2.70)	(32.0)	(0.43)	(0.29)	(<0.03)	(<0.02)	(<0.01)	(<0.05)
6	1.40	13.0	0.63	0.39	–	0.01	–	–
	(12.0)	(12.0)	(0.63)	(0.39)	(<0.03)	(<0.02)	(<0.01)	(<0.05)
7	1.43	15.7	0.37	0.10	–	–	–	–
	(12.0)	(9.40)	(0.36)	(0.10)	(<0.03)	(<0.02)	(<0.01)	(<0.05)

^aMeasured values are listed in parentheses on the second line. The values for O VI, C III, and H I are from Kriss et al. (2000).

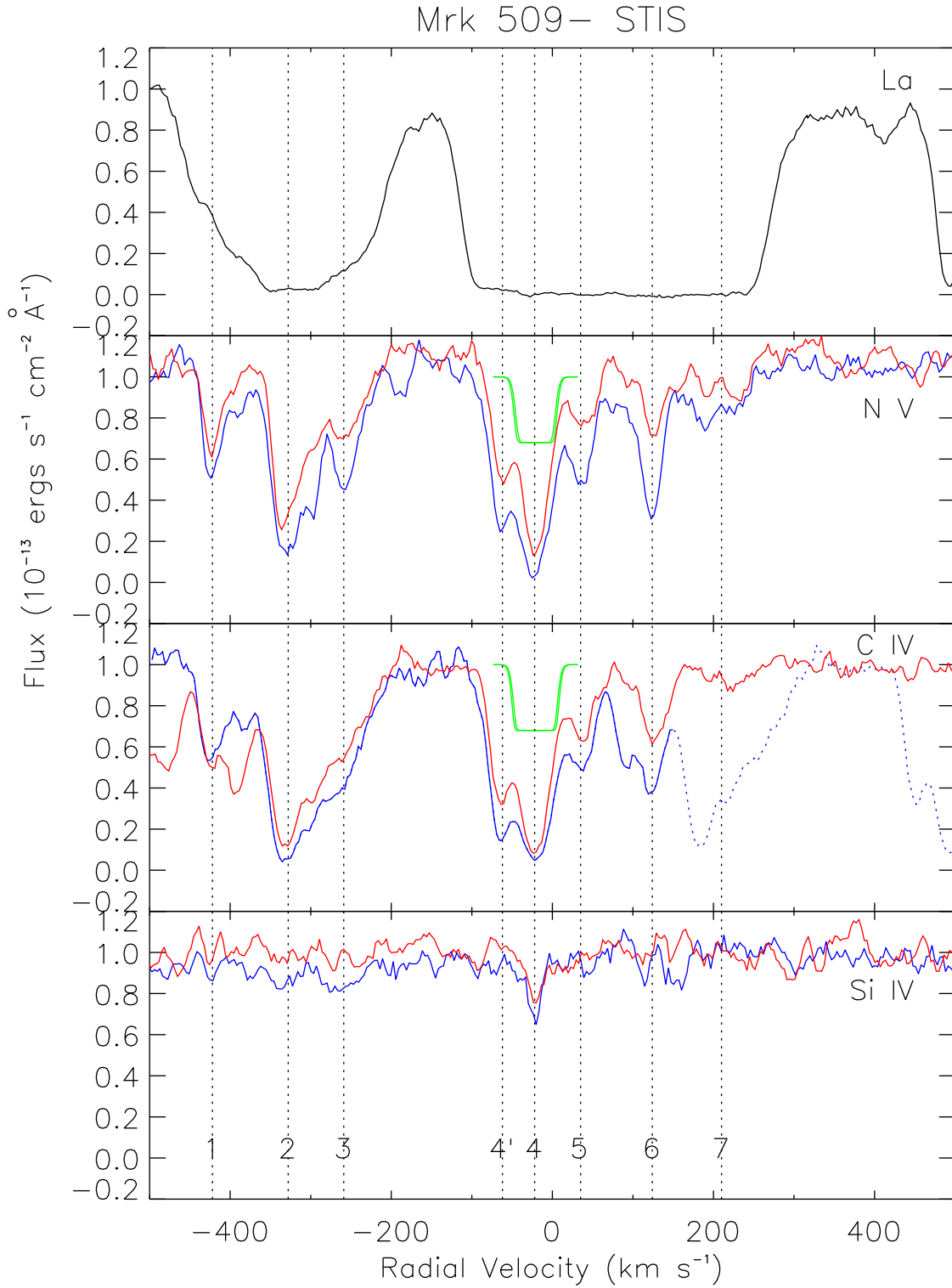


Fig. 1.

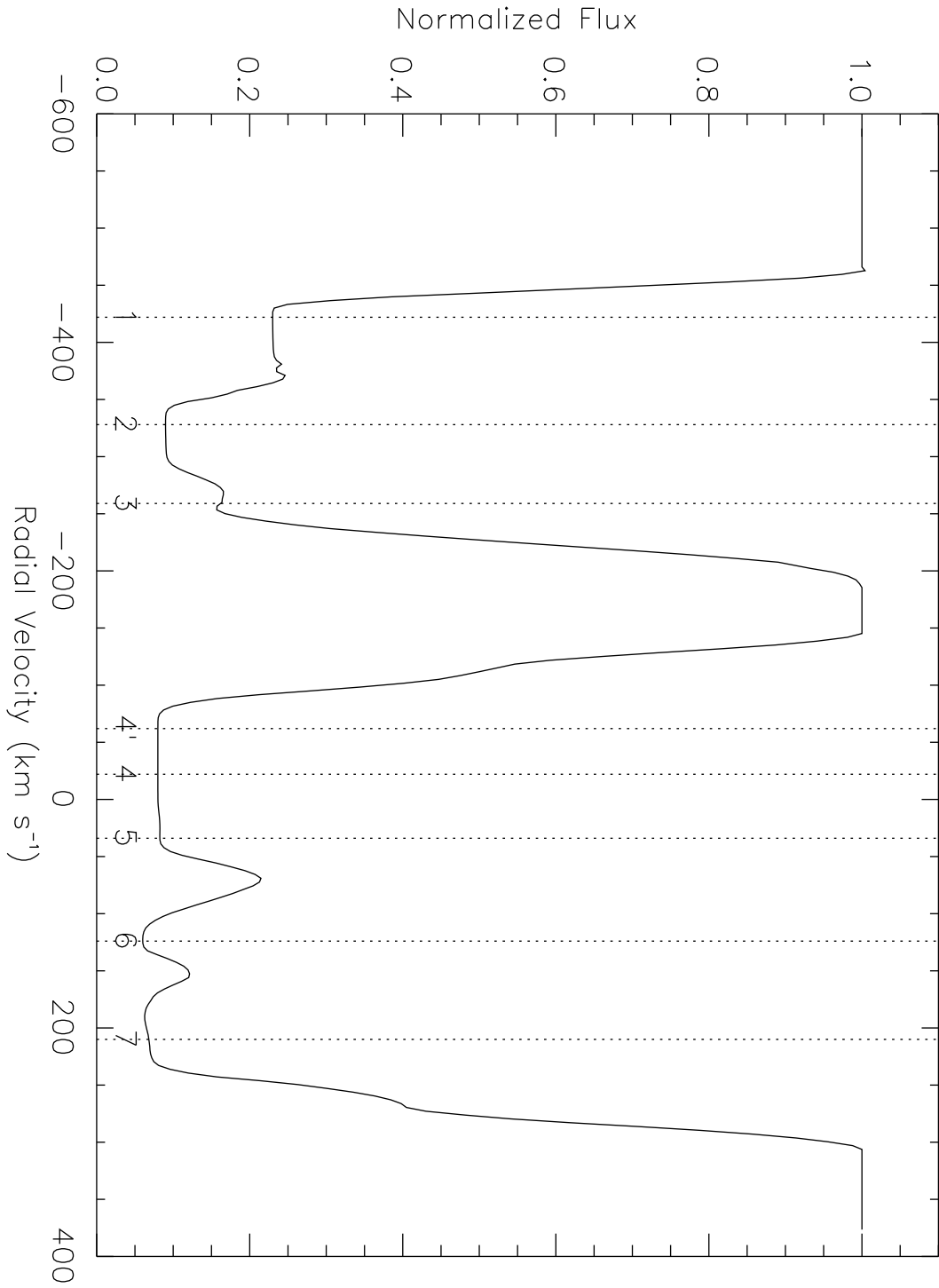


Fig. 3.